TOPICAL REVIEW

# Semiconductor–superconductor optoelectronic devices



IOP Publishing Journal of Optics
J. Opt. 19 (2017) 103003 (16pp) https://doi.org/10.1088/2040-8986/aa8888

Topical Review

# Semiconductor–superconductor optoelectronic devices

**Shlomi Bouscher, Dmitry Panna and Alex Hayat**[1]

Department of Electrical Engineering, Technion, Haifa 32000, Israel

E-mail: alex.hayat@ee.technion.ac.il

Received 12 July 2016, revised 9 August 2017
Accepted for publication 25 August 2017
Published 20 September 2017


**Abstract**

Devices combining superconductors with semiconductors offer a wide range of applications, particularly in the growing field of quantum information processing. This is due to their ability to take advantage of both the extensive knowledge gathered in the field of semiconductors and the unique quantum properties of superconductors. This results in novel device concepts, such as structures generating and detecting entangled photon pairs as well as novel optical gain and laser realizations. In this review, we discuss the fundamental concepts and the underlying physical phenomena of superconductor–semiconductor optoelectronics as well as practical device implementations.

Keywords: semiconductors, superconductors, optoelectronics

(Some figures may appear in colour only in the online journal)

## 1. Introduction

Semiconductors have been at the core of solid-state physics research for more than half a century as a major driving force of technology since the invention of the transistor and the laser diode. The amount of research done in semiconductor physics [1] has been nearly matched by the attempts to understand and manipulate the solid-state quantum-condensate phenomenon of superconductivity [2]. Superconductors enable the realization of broadband ultrafast single-photon detectors [3, 4] as well as one of the most promising approaches to the implementation of quantum computing [5, 6]. Combining these two material families [7, 8] can open a wide range of possible directions in basic research and in technological applications [9–14]. Hybrid semiconductor–superconductor devices, which take advantage of both the mature technology and controllability of semiconductor structures and the collective quantum states of superconductors, have been attracting growing attention lately [13, 14]. As a consequence, a new interdisciplinary field of superconducting optoelectronics, based on the interaction of light with semiconductor–superconductor structures has emerged. Hybrid light-emitting diodes [15, 16] exhibit emission enhanced by the superconducting state [17, 18], while novel superconductor based lasers [19] and quantum light sources have been proposed [20, 21].

The phenomenon of superconductivity, where certain materials exhibit zero resistance below a critical temperature $T_c$, has been known for over a century. The behavior of conventional low-temperature (low-$T_c$) superconductors has been successfully described by the Bardeen–Cooper–Schrieffer (BCS) theory [2]. According to this model, at temperatures below $T_c$ electrons form entangled Cooper pairs with bosonic nature. Electron Cooper pairing enables the formation of a collective macroscopic quantum state—a condensate, with the order parameter $\Delta$, related to Cooper pair binding energy, appearing as the superconducting gap in the density of states. This quantum condensation phenomenon gives rise to several unique properties which distinguish superconductors from other materials, such as the ability to conduct current without resistance, the expulsion of magnetic fields from superconductors via the Meissner effect and quantization of magnetic flux [2]. Tunneling of the macroscopic condensate through insulators, normal materials or weak links in the Josephson effect [37] allows the realization of superconducting quantum interference devices (SQUID) that are able to detect extremely weak magnetic fields. On the other hand, the electron entanglement in

[1] Author to whom any correspondence should be addressed.

 

individual Cooper-pairs can be exploited for various quantum information processing applications including quantum light sources [36] and entangled photon detectors [47].

This paper is structured as follows. We start with hybrid devices incorporating p–n junctions (section 2) including either one or two superconducting contacts. We then proceed to discuss two additional applications based on superconducting p–n junctions which are superconductor coupled waveguides (section 3) and the photonic Bell-state analyzer (section 4). Quantum dot (QD) based hybrid devices are then discussed (section 5) along with a possible application in the form of Josephson lasers (section 6). This is followed by concluding remarks (section 7).

## 2. P–n junction superconducting light sources

P–n junctions have long been used as light emitting diodes (LEDs) with the first-order light–matter interaction leading to electron–hole recombination as the source of both spontaneous photon emission in LEDs for illumination and as quantum light sources [22], as well as stimulated emission processes at the core of semiconductor lasers [23], enabling modern telecommunication and metrology. Second-order two-photon emission processes in conventional semiconductor structures are significantly weaker—by nearly 5 orders of magnitude [24–29] compared to the first-order one-photon emission process. Since superconductivity is based on electron Cooper-pairs [2], hybrid structures combining superconductors with semiconductors (such as the p–n junction) can exhibit much stronger two-photon emission based on second-order light–matter interaction involving Cooper-pairs. Such second-order light–matter interactions in semiconductor–superconductor structures have been shown, both theoretically [17] (equation (5)) and experimentally [16, 30–32] to be the underlying physical effect behind enhanced luminescence obtained in superconducting LEDs (SLEDs) at temperatures lower than $T_c$.

In semiconductor–superconductor optoelectronic devices, superconductivity is induced locally in the semiconductor structure by injection of Cooper pairs from the superconducting contacts via the proximity effect [33], such that a thin layer of the semiconductor structure itself becomes superconducting with electrons in the conduction band paired in Cooper pairs (figure 1). The origin of this phenomenon lies in the Cooper-pair transport through the superconductor–semiconductor interface. Since Cooper-pairs are found at the Fermi level of the superconductor, the adjacent semiconductor has to be n-doped to the level of degeneracy ($n^{++}$ layer), for its Fermi level to reside inside the conduction band, thus allowing Cooper-pair injection from the superconductor. Once a small voltage is applied to the superconductor–semiconductor junction, Cooper-pairs are injected into the heavily doped n-type semiconductor, proceeding to the p–n junction, where they undergo recombination with holes, resulting in photon pair emission (figures 1 and 2(a)).

An important device parameter to consider is the strength of the barrier (e.g. Schottky barrier) at the semiconductor–superconductor interface, which determines the probability of

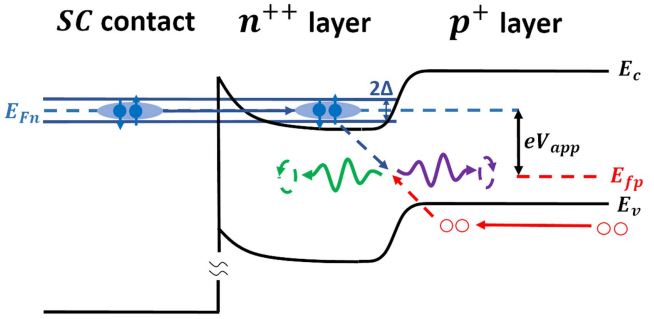


**Figure 1.** A schematic drawing of Cooper pair (blue) injection from a superconductor into a semiconductor p–n junction resulting in photon pair emission by recombination with holes (red). $E_C$ and $E_V$ denote the semiconductor conduction and valence band edges respectively. $2\Delta$ is the superconducting gap, $E_{\rm fn}$ and $E_{\rm fp}$ are the electron and hole quasi-Fermi levels respectively and $V_{\rm app}$ is the applied voltage on the device.

Cooper-pair injection into the semiconductor. Highly doped semiconductors also reduce the Schottky barrier thickness [34], thus enhancing Cooper-pair injection.

The theoretical basis of Cooper-pair based photon-pair emission in semiconductors lies in the second-order perturbation expansion for the light–matter interaction in the superconducting BCS state of electrons, where the Hamiltonian of the interaction is given by [17]:

$$\hat{H}_I = \sum_{k,q,\sigma} B_{k,q}\hat{b}_{q-k,\sigma}\hat{c}_{k,\sigma}\hat{a}_q^{\dagger} + \text{h.c.}, \tag{1}$$

where $B_{k,q}$ is the electron–photon coupling energy (interaction strength), $k$, $q$ represent momenta, $\sigma$ is the spin, $\hat{b}$ is the hole annihilation operator, $\hat{c}$ is the electron annihilation operator and $\hat{a}^{\dagger}$ is a photon creation operator. The interaction Hamiltonian $\hat{H}_I$ describes the fundamental quantum-electrodynamics (QED) interaction, in which an electron and a hole are annihilated producing a single photon. The recombination of an electron Cooper *pair* with a *pair* of holes is described by a second-order perturbation calculation—resulting in the emission of a photon *pair*. The second-order term of the perturbation involves the product of two interaction Hamiltonian operators $|\chi_t(2)\rangle = -\int_{-\infty}^{t} \mathrm{d}t' \int_{-\infty}^{t'} \mathrm{d}t'' \hat{H}_I(t')\hat{H}_I(t'')|\chi_i\rangle$. Therefore, all relevant operators appear twice, including the photon creation operator. Such higher-order multiphoton process in the fundamental QED Hamiltonian [49] can be described phenomenologically by a first-order process in an effective interaction Hamiltonian [35], as often done in quantum nonlinear optical processes such as parametric down conversion. The initial state is given by:

$$|\chi_0\rangle = |0\rangle|N\rangle|P\rangle, \tag{2}$$

where $|0\rangle$ denotes the photon vacuum state, $|N\rangle$ denotes the conduction band BCS state and $|P\rangle$ denotes the valence band hole state. Using the photon number operator, $\hat{N}_{\rm ph} \triangleq \sum_q \hat{a}_q^{\dagger}\hat{a}_q$, the number of emitted photons to the first and second order is:

$$\langle\hat{N}_{\rm ph}\rangle = \langle\hat{N}_{\rm ph}(1)\rangle + \langle\hat{N}_{\rm ph}(2)\rangle, \tag{3}$$

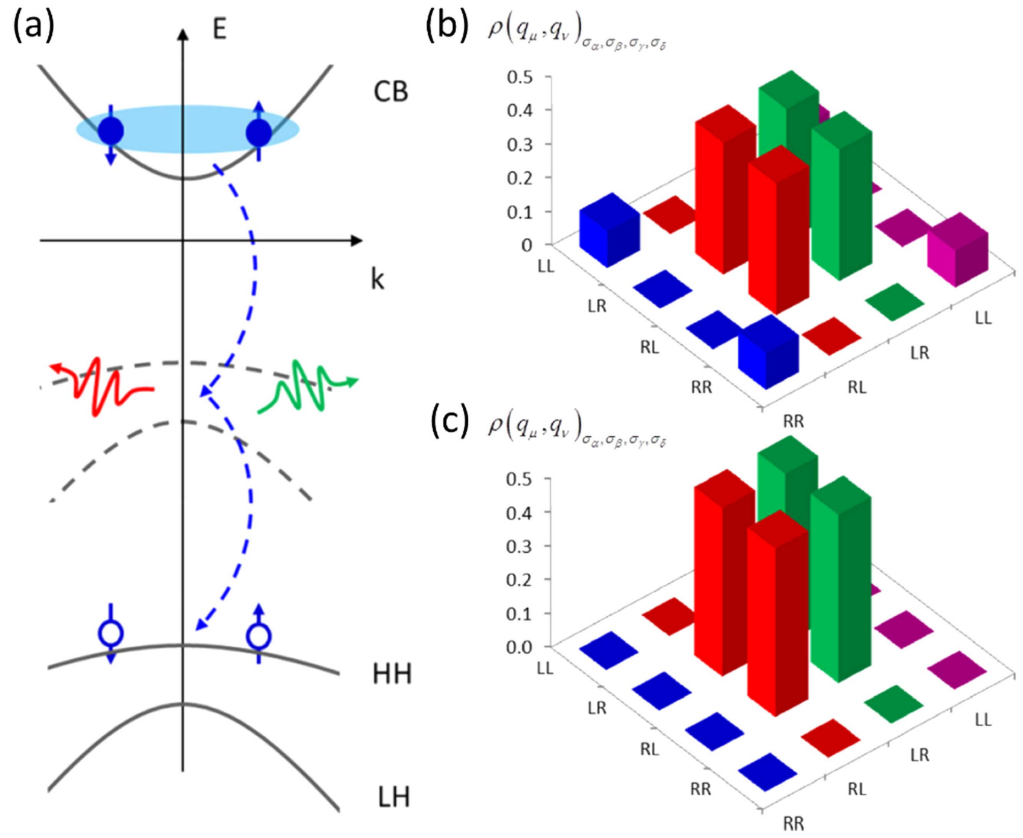


**Figure 2.** (a) Cooper-pair based photon pair emission diagram. Note that the recombination is a second order process as no single electron states are found inside the superconducting gap. (b), (c) Calculated density matrix of the two-photon polarization state for Cooper-pair luminescence (b) in a bulk semiconductor and (c) in a QW with large LH–HH splitting. Reprinted figure with permission from [36], Copyright 2014 by the American Physical Society.

where:

$$\langle \widehat{N}_{\rm ph}(1)\rangle = \int_{-\infty}^{t} {\rm d}t_1 \int_{-\infty}^{t} {\rm d}t_2 \langle \chi_0 | \widehat{H}_I(t_1)\widehat{N}_{\rm ph}\widehat{H}_I(t_2)|\ \chi_0\rangle$$

$$\langle \widehat{N}_{\rm ph}(2)\rangle = \int_{-\infty}^{t_2} {\rm d}t_1 \int_{-\infty}^{t} {\rm d}t_2 \int_{-\infty}^{t} {\rm d}t_3 \int_{-\infty}^{t_3} {\rm d}t_4 \times \langle \chi_0 | \widehat{H}_I(t_1)\widehat{H}_I(t_2)\widehat{N}_{\rm ph}\widehat{H}_I(t_3)\widehat{H}_I(t_4)|\ \chi_0\rangle. \quad (4)$$

Explicit calculation [17] of the second-order contribution yields (with natural units),

$$\overline{\langle \widehat{N}_{\rm ph}(2)\rangle} = 4\pi\,|B|^4 \sum_{q,\sigma}\delta(\Omega_{k_F,q})\sum_k \left[\frac{f_k^n(1-f_k^n)}{(E_k - {\rm i}/\tau)^2} + \frac{f_k^n(1-f_k^n)}{(E_k + {\rm i}/\tau)^2} + \frac{(f_k^n)^2 + (1-f_k^n)^2}{E_k^2 + ({\rm i}/\tau)^2}\right]\frac{\Delta^2}{E_k^2} \quad (5)$$

with the Fermi–Dirac distribution $f_k^n = [1 - \tanh(E_k/2T)]/2]$, $E_k = \sqrt{\left(\frac{k^2}{2m} - \mu_n\right)^2 + \Delta^2}$, and $\tau$ is the relaxation time. The interaction strength $|B|^2$ is squared in the second-order process and the Fermi–Dirac distribution for both valence-band and conduction-band appear twice to account for two conduction-band quasiparticles $f_k^n$ and two valence-band quasiparticles $f_k^p$. The valence band hole Fermi–Dirac distribution is assumed to be $f_k^p = 1$ in the relevant energy range due to the low temperatures required for superconductivity. Since annihilation operators of conduction-band quasiparticles in the superconducting state are linear combinations of both creation and annihilation of electrons in the Bogoliubov transformation [2], all combinations of products of $f_k^n$ and $(1 - f_k^n)$ appear in the four terms in the expression. The corresponding quasiparticle energy resonant levels appear in the denominators, resulting from the 2nd order perturbation calculation, with a broadening term $\tau$. $\delta(\Omega_{k_F,q})$ describes the energy conservation condition, and the factor $\Delta^2$ shows the relation of the superconducting order parameter $\Delta$ to the enhanced emission. This calculation predicts luminescence enhancement for temperatures below $T_c$ ($T < T_c$), and it agrees with the recent experimental results (figure 3) [16].

Moreover, it has been shown theoretically, that the photon pairs emitted from semiconductor quantum wells (QWs) in proximity to a superconductor contact can be polarization-entangled [36] (figures 2(b) and (c)), enabling a practical quantum light source. Unlike quantum light sources based on isolated emitters such as single atoms or QD [22], Cooper-pair recombination in semiconductors is not based on spin population in discrete energy levels, but rather on Cooper-paired inherently entangled electrons in a continuum of states emitting entangled photon pairs. Electrons in Cooper pairs are entangled through their spins, and their recombination with holes in semiconductors can map this electron entanglement into entanglement of the emitted photon pairs' circular polarization—in a properly designed structure

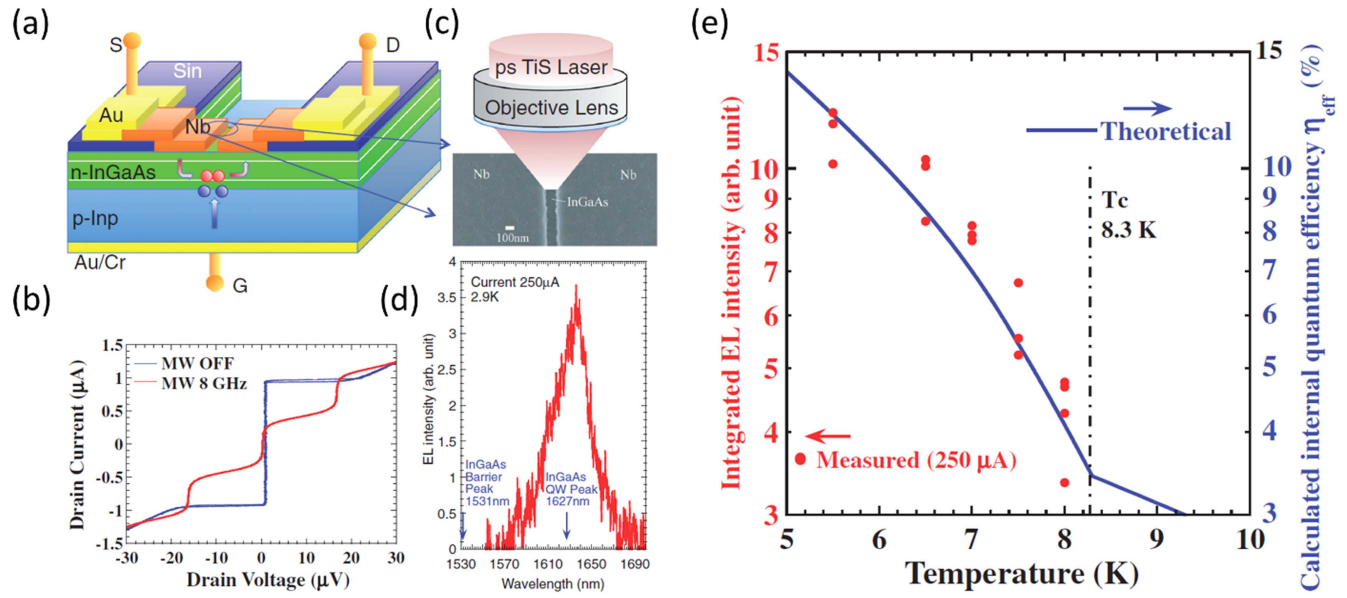


**Figure 3.** (a) A typical structure of a p–n based SLED. The n-type layer is heavily doped in order to allow Cooper-pair penetration into the junction. Due to the close proximity of the Nb contacts to each other, the above device also displays the characteristics of a Josephson junction. (b) Current–voltage plot with and without applied microwave radiation. The device displays the typical current–voltage characteristics of a Josephson junction as well as the effect of Shapiro steps. (c) The fabrication method employed in creating the gap between the Nb electrodes. (d) Electroluminescence (EL) intensity spectrum of the device. A clear peak is evident which results from the InGaAs QW. (e) Integrated EL intensity and quantum efficiency for various temperatures. An increase of EL intensity is observed for temperatures lower than $T_c$. Reproduced from [16]. 

(figure 2(a)). In addition, since no single-electron states are allowed in the superconducting gap $2\Delta$, the Cooper-pair recombination with holes is a second-order process and not a cascade of first-order processes—thus leaving no which-path information and enabling pure entangled photon state generation. Furthermore, it is important to note that two-photon absorption and emission are second-order processes in the quantum perturbation theory, however they are linked to the third-order nonlinear susceptibility by the nonlinear Kramers–Kronig relations [49].

The Hamiltonian describing the interaction which leads to this Cooper-pair based photon entanglement is a modified version of the previous Hamiltonian (equation (1)), including spin–orbit coupled charge-carrier angular momentum $J$ and photon polarization $\sigma$:

$$\widehat{H}_I = \sum_{k,q,\sigma,J} B_{k,q}\hat{b}_{-(k-q),-J}\hat{c}_{k,J}\hat{a}^{\dagger}_{q,\sigma} + \text{h.c.} \tag{6}$$

The obtained density matrix describing the polarization state of the emitted photon-pairs (with HH band electrons) is:

$$\begin{aligned}\rho(q_\mu, q_\nu)_{\sigma_\alpha,\sigma_\beta,\sigma_\gamma,\sigma_\delta} &= \langle\chi_t|\hat{a}^{\dagger}_{q_\mu,\sigma_\alpha}\hat{a}^{\dagger}_{q_\nu,\sigma_\beta}\hat{a}_{q_\mu,\sigma_\gamma}\hat{a}_{q_\nu,\sigma_\delta}|\chi_t\rangle \\ &= \int_{-\infty}^{t} dt_1 \int_{-\infty}^{t_1} dt_2 \int_{-\infty}^{t} dt_3 \int_{-\infty}^{t_3} dt_4 \\ &\times \langle\chi_0|\widehat{H}_I(t_1)\widehat{H}_I(t_2)\hat{a}^{\dagger}_{q_\mu,\sigma_\alpha}\hat{a}^{\dagger}_{q_\nu,\sigma_\beta}\hat{a}_{q_\mu,\sigma_\gamma} \\ &\times \hat{a}_{q_\nu,\sigma_\delta}\widehat{H}_I(t_3)\widehat{H}_I(t_4)|\chi_0\rangle.\end{aligned} \tag{7}$$

In bulk direct-bandgap semiconductors the light-hole (LH) and heavy-hole (HH) bands with different charge-carrier angular momentum are degenerate close to Brillouin zone center. This in turn causes degradation of the entanglement as there are several decay paths with different polarizations of the emitted photons, thus resulting in a certain level of mixing of the entangled photon states with density matrix given by:

$$\rho(q_\mu, q_\nu) = \alpha\rho(q_\mu, q_\nu)^{\text{HH}} + \beta\rho(q_\mu, q_\nu)^{\text{LH}}, \tag{8}$$

where the coefficients $\alpha$, $\beta$ depend on the population of the bands.

Such degeneracy, however, can be lifted by using a semiconductor QW, which induces a split between the LH and HH bands. The induced split is an important parameter of the purity of the obtained entangled photon-pair state (figures 2(b) and (c)). This, together with emission rate enhancement for $T < T_c$, can result in efficient sources of entangled photon-pairs.

We now turn our attention to two distinct SLED structure types: one containing a single superconductor contact (coupled to the n-type layer) and another, containing two superconducting contacts for both n and p-type layers of the p–n junction.

### *2.1. SLEDs with a superconducting contact on n-type side only of the p–n junction*

The first type of SLED structure with only n-type side of the p–n junction connected to a superconductor contact, has been implemented and thoroughly explored [16, 30–32]. The typical structure is composed of a p–n junction with two

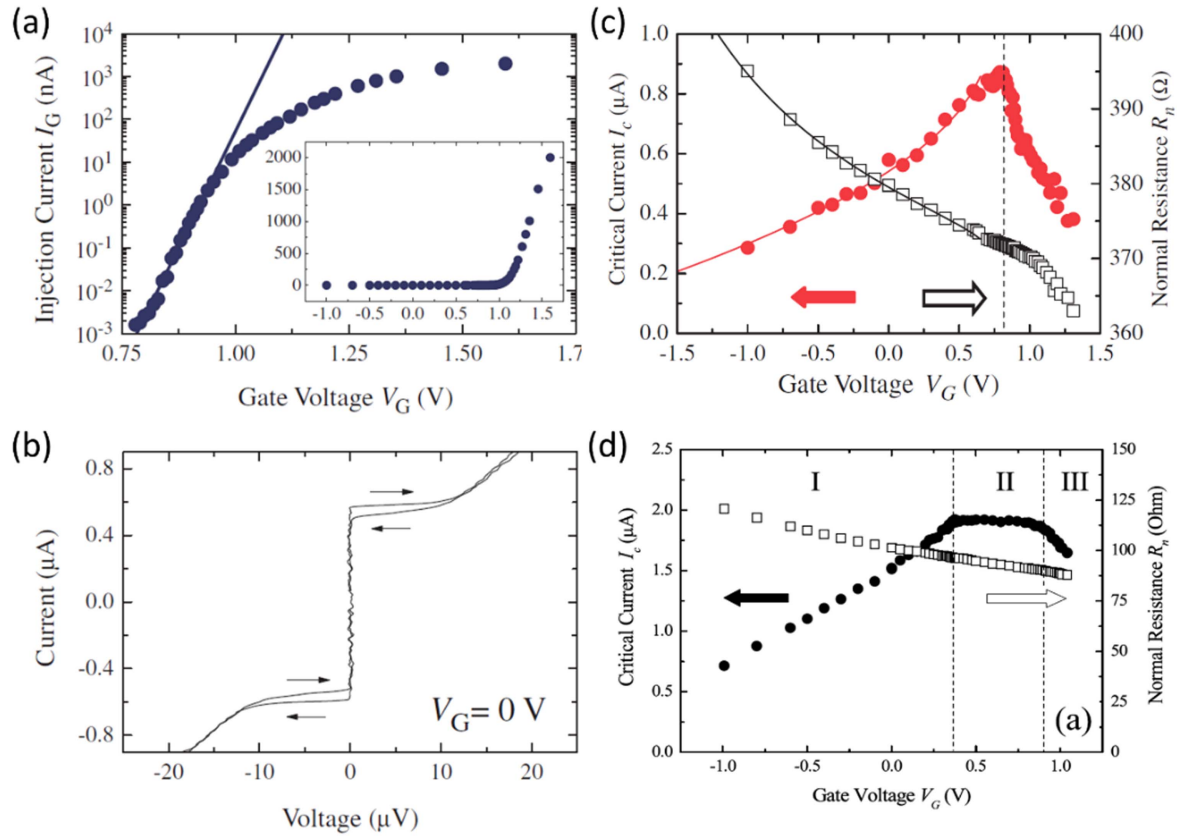


**Figure 4.** (a) Current–voltage (*IV*) characteristic of the p–n junction. (b) *IV* characteristic of the top Josephson junction with zero gate voltage. (c), (d) *IV* characteristics of the critical current versus applied voltage for two devices with similar dimensions but different doping: the device in (c) having stronger n-type doping than device in (d). Device (d) also lacks the moderate gating voltage region with the constant critical current. Reproduced from [30, 32]. © 2014 The Japan Society of Applied Physics. All rights reserved.

superconducting contacts placed on top of the n-type layer (figure 3(a)). The two contacts on the n-type side of the p–n structure form a Josephson junction which enables probing superconductivity via the Josephson effect. Josephson junctions are made of a normal material between two superconductors [37], where the normal material is thin enough so that the macroscopic wave-functions of each superconducting condensate overlap and are therefore coupled. This coupling gives rise to the Josephson effect, where both the voltage $V(t)$ and current $I(t)$ across the Josephson junction are related to the phase difference $\phi(t)$ between the two superconducting condensates according to [37]:

$$V(t) = \frac{\hbar}{2e}\frac{\partial\phi(t)}{\partial t},$$
$$I(t) = I_c \sin(\phi(t)), \tag{9}$$

where $I_c$ is the critical current of the junction. These relations are at the core of both the dc Josephson effect, with dc current across the junction without any applied voltage, as well as the ac Josephson effect, which results in oscillating current with application of constant voltage.

In the implemented SLED devices, which include Josephson junctions, the distance between the superconducting contacts has been made small enough (on the order of ∼100–200 (nm)) for a significant Josephson effect on the top layer of the device. The Josephson behavior is evident through both the current–voltage (*I*–*V*) characteristics [16, 31, 32] (figures 3(b) and 4(b)), and the effects induced by microwave irradiation of the junction [16, 31], which manifest as frequency-dependent critical current and Shappiro steps [16, 31] (figure 3(b)). Moreover, the substrate itself can be gated, thus forming a Josephson field effect transistor (JoFET) in which the critical current and normal resistance can be controlled using the gate voltage. Since the gate is not insulated from the conductive channel as in regular MOSFET devices, application of gate voltage also induces a small current from the gate $I_G$ whose behavior matches that of a p–n junction (figure 4(a)).

For low gate voltages $V_G$ below ∼0.75 V, this control is obtained through modulation of the depletion layer in the p–n junction and the subsequent increase or decrease of the cross-section in the supercurrent. This dependence is summarized in the following set of equations:

$$I_c = \frac{en_p\hbar}{m^*}\frac{W[H - x(V_G)]}{L},$$
$$R_n = R_0 + \frac{1}{en_q\mu}\frac{L}{W[H - x(V_G)]},$$
$$x(V_G) = x(0)\sqrt{1 - V_G/V_i}, \tag{10}$$

where $L$, $H$, $W$ are the length, thickness and width of the junction, $R_0$ is the interfacial resistance, $m^*$ is the effective electron mass $x(0)$, $V_i$ are fitting parameters, $x(V_G)$ is the thickness of the depletion region and $n_q$, $n_p$ are the quasi-particle and superconducting pair densities respectively. The above equations have

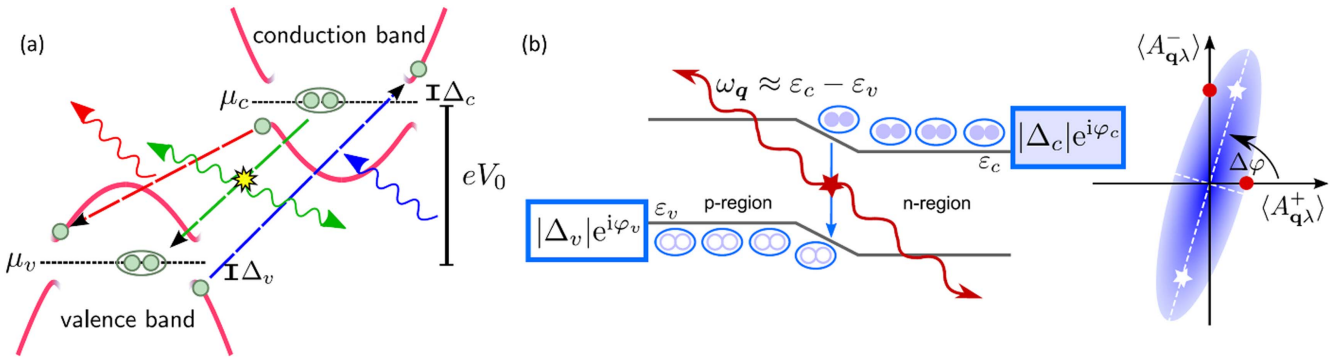


**Figure 5.** (a) Energy band diagram of a second type SLED under applied voltage $V_0 = \mu_c - \mu_v$ where $\mu_c$, $\mu_v$ are the conductance and valence band quasi fermi levels respectively and $\Delta_v$, $\Delta_c$ are the superconducting gap values each side. Three key processes can be observed: (1) transfer of a quasi-particle from the conduction band to the valence band with a 'red' photon emission with energy $\omega_q \leqslant eV_0 - |\Delta_c| - |\Delta_v|$. (2) Transfer of a quasiparticle from the valence band to the conduction band and the absorption of a 'blue' photon with energy $\omega_q \geqslant eV_0 - |\Delta_c| - |\Delta_v|$. (3) Cooper pair tunneling through recombination/emission of two 'green' photons with energy $\omega_q = eV_0$. (b) Cooper pair recombination and entangled photon-pair emission. The electronic coherence of the Cooper-pairs is transferred to the photons, thus leading to a two-mode squeezing of the quadrature operators $\hat{A}^{\pm}_{q\lambda}$ through control of the relative phase between the superconducting contacts $\Delta\varphi = \varphi_c - \varphi_v$. The emitted entangled photon-pairs have energies $\omega_q = \varepsilon_c - \varepsilon_v$. (a) Reprinted figure with permission from [39], Copyright 2015 by the American Physical Society. (b) Reprinted figure with permission from [38], Copyright 2014 by the American Physical Society.

been shown to match the behavior of the device for voltages lower than ~0.75 V (figure 4(c)).

For gate voltages higher than ~0.75 V, a decrease in the critical current has been observed (figure 4(c)). This decrease is attributed to non-equilibrium photo-generated carriers at the p–n junction due to the gate current. The photons are absorbed in the channel region, generating hot electrons, which then proceed to form a large concentration of quasiparticles from broken Cooper-pairs. In addition, for similar devices with a slightly lower doping [31, 32], a third transition region, in which the critical current becomes constant at a certain range of gate voltages below those reducing the critical current, has also been observed (figure 4(d)), and is attributed to the increase in non-equilibrium charges due to photon absorption by Cooper-pairs.

The obtained result is that a weak gate current injection on the order of a few pA can modulate the much stronger critical current which is on the order of several $\mu$A, so that such a device has a very high current monitoring sensitivity. Moreover, the transport characteristics have been shown to be modulated in three distinct types of regimes. In the gate control regime, almost no current is being injected from the gate electrode into the p-type side with the Josephson junction's characteristics being modified through the field effect alone, in which both quasi-particles and Cooper-pairs tunnel through the junction. In the radiative recombination regime, high recombination efficiency has been demonstrated. Finally, in the carrier injection regime, the critical current is reduced due to photon absorption by Cooper-pairs.

### *2.2. SLEDs with superconducting contacts on both n-type and p-type sides of the p–n junction*

The proposals of the second type of SLED with superconducting contacts on both n-type and p-type sides of the SLED which, while not yet demonstrated experimentally, offer interesting directions on potential devices [38, 39], based on the phase difference between the superconducting contacts, in a manner similar to that of the Josephson junction. The phase difference has been theoretically shown to result in quantum squeezing in the quadrature amplitudes of the emitted light. The overall Hamiltonian, which is similar to the Hamiltonian of a quantum parametric amplifier [38], is

$$\widehat{H} = \omega\hat{a}^{\dagger}\hat{a} + \xi e^{-ieV_0 t}\hat{a}^{\dagger} + i\gamma e^{-2ieV_0 t}\hat{a}^{\dagger}\hat{a}^{\dagger} + \text{h.c.}, \qquad (11)$$

where $\hbar$, $c = 1$, $\hat{a}^{\dagger}$, $\hat{a}$, are the photon creation and annihilation operators respectively, $\xi$, $\gamma$ are the one-photon and two-photon emission process amplitudes respectively, $\omega$ is the photon frequency and $V_0$ is the applied voltage between the contacts. It has been shown that $\gamma \sim |\Delta_v||\Delta_c|\, e^{i\Delta\varphi}$ where $|\Delta_v|$, $|\Delta_c|$ are the superconducting gap values for each of the superconductor contacts and $\Delta\varphi$ is the phase difference between the superconductor phases on each side of the contact (figure 5). Thus, the phase difference is related directly to the pair generation amplitude $\gamma$, allowing control of quantum squeezing of light emitted from the device [40]. Moreover, since both sides of the p–n junction are heavily doped to the point of degeneracy, when no voltage is applied to the junction, the Fermi level lies above the bottom of the conduction band in the n-type side and below the top of the valence band in the p-type side—similar to the configuration in the Esaki diode [41]. Similarly, when voltage is applied to the junction, the quasi Fermi levels reside within their respective bands on each side of the junction. As a result, the difference between the Fermi levels (the applied voltage) becomes the important parameter determining carrier energies and emitted photon wavelengths rather than the width of the bandgap.

The phase difference can be controlled through the voltage applied to the SLED, thus theoretically allowing not only generation of photon-pairs, but also electrical control over the squeezing angle of the squeezed two-photon state.

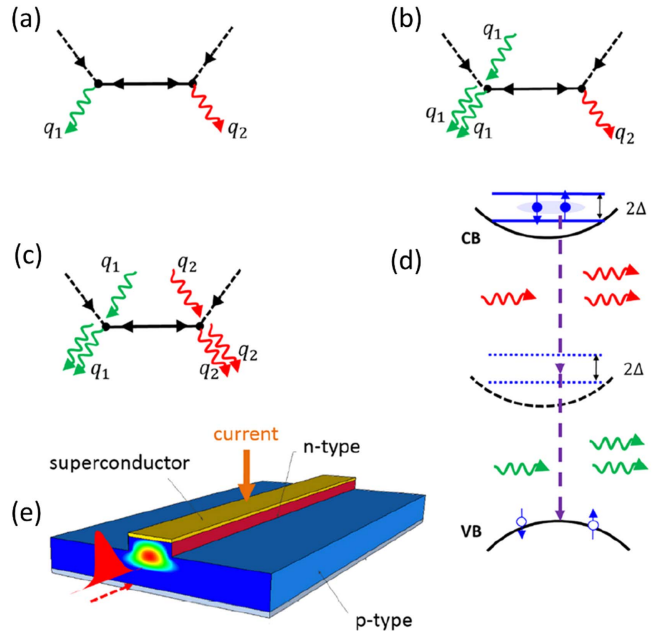


**Figure 6.** (a)–(c) Feynman diagram of spontaneous/partially-stimulated/fully-stimulated two-photon emission. (d) Energy level diagram for the fully stimulated two-photon emission process. (e) The proposed superconductor-coupled waveguide structure. Reproduced from [42] © 2016 IOP Publishing Ltd and Deutsche Physikalische Gesellschaft. CC BY 3.0.

## 3. Superconductor-coupled waveguides

In addition to enabling entangled-photon pair generation, semiconductor–superconductor based structures have been also proposed as highly efficient two-photon amplifiers [42].

While two-photon gain (TPG) has been studied in conventional semiconductor structures [43–46], hybrid semiconductor–superconductor structures have been shown to yield a broadband enhancement of the ultrafast two-photon amplification. Moreover, it has been shown that for a seed pulse with moderately high intensity, the contribution from the superconductor-enhanced TPG approaches that of the one-photon gain (OPG). Such superconductor–semiconductor TPG structures can be obtained by combining a semiconductor waveguide with a superconducting top contact. Applying current to the superconducting contact results in Cooper-pair injection into the semiconductor p–n structure based waveguide.

These Cooper-pairs can then take part in one of three processes: the first is spontaneous two-photon-emission (TPE) (figure 6(a)) in which the Cooper-pair recombines with two holes to emit a pair of photons spontaneously. The second process is singly-stimulated TPE (figure 6(b)) in which a single photon interacts with the Cooper-pair causing a partially stimulated emission of two photons, and the third process is the fully stimulated TPE, in which a photon pair interacts with the Cooper-pair and causes a full stimulated emission of two photons (figure 6(c)), resulting in TPG.

The expression for the ratio between the TPG—$g^{(2)}$ and OPG—$g^{(1)}$ has been derived for the low temperature limit $T \to 0$ in the high intensity ($|\alpha_q| \gg 1$) regime, where $|\alpha_q|^2$ is the average photon number in the coherent state describing the seed pulse:

$$\frac{g^{(2)}}{g^{(1)}} = \widetilde{C}\left|\frac{B\alpha_q\Delta}{\Omega}\right|^2 \times \frac{1-\Theta(2\omega_q-2\widetilde{\mu}_n)}{\Theta(2\widetilde{\mu}_n-\omega_q)\Theta(\omega_q-2\widetilde{\mu}_n+\mu_n)-\Theta(\omega_q-2\widetilde{\mu}_n)},$$
$$\widetilde{C} = 4m_n(\mu_n-\Delta+\sqrt{\mu_n^2+\Delta^2})\Big/m_p\mu_p[(\omega_q-\widetilde{\mu}_n)^2+\Delta^2],$$
$$\widetilde{\mu}_n = E_c+\frac{eV_{\text{app}}}{2}+\mu_n \quad \Omega = \omega_q-\varepsilon_p(k-q)-\widetilde{\mu}_n, \tag{12}$$

where $m_n$, $m_p$ are the electron/hole effective masses, $\mu_n$, $\mu_p$ are the electron/hole quasi-fermi levels, $2\Delta$ is the superconducting gap, $\omega_p$, $\varepsilon_p$, $\varepsilon_n$ are the photon/hole/electron energies, $k$, $q$ are wave numbers, $B$ is the coupling energy, $E_c$ is the conduction band edge and $V_{\text{app}}$ is the applied voltage. The ratio is proportional to $|B\alpha_q\Delta|^2$ showing that TPG is favored for large intensities (figure 7). This is because the second-order $g^{(2)}$ term involves the square of the interaction strength $|B|^2$, and is proportional to $|\alpha_q|^2$, while the first-order $g^{(1)}$ term involves $|B|^2$ once and does not depend on $|\alpha_q|^2$. The denominator $\Omega = \omega_q - \varepsilon_p(k-q) - \tilde{\mu}_n$ contains the resonant condition of the second-order perturbation calculation. In addition, since both $g^{(1)}$ and $g^{(2)}$ are calculated at zero temperature, the Fermi–Dirac distributions of the charge carriers are represented by the set of Heaviside functions $\Theta$ shifted to corresponding energies. The energy scale in this calculation is relative to the top of the valence band $E_v$, so that $E_c$ effectively represents the semiconductor bandgap.

The carrier thermalization time in superconductors is on the scale of several tens of ps and the Cooper-pair breaking time is on the scale of several ps, both being much longer than the duration of the laser pulse, thus guaranteeing proper operation of the proposed device. Moreover, the predicted energy of the laser pulse is on the pJ scale which is several orders of magnitude smaller than ionization intensities. Therefore, such devices have important implications in the field of optoelectronics and in coherent-control applications.

## 4. Photonic Bell-state analyzer based on a superconductor–semiconductor device

Superconductor–semiconductor hybrid structures have been proposed for projective measurements of maximally entangled-photon states, also known as Bell-states [47], with numerous applications in quantum technologies such as quantum computing [48, 50, 51] and quantum teleportation [52–54]. The four Bell-states can be implemented by polarization-entangled photons:

$$|\Psi^{\pm}\rangle = \frac{1}{\sqrt{2}}(|R\rangle_{\omega_\mu}|L\rangle_{\omega_\nu} \pm |L\rangle_{\omega_\mu}|R\rangle_{\omega_\nu}),$$
$$|\Phi^{\pm}\rangle = \frac{1}{\sqrt{2}}(|R\rangle_{\omega_\mu}|R\rangle_{\omega_\nu} \pm |L\rangle_{\omega_\mu}|L\rangle_{\omega_\nu}), \tag{13}$$

where $|R\rangle$, $|L\rangle$ denote right and left circular photon polarizations respectively and $\omega_\mu$, $\omega_\nu$ denote the photon energies. However, it has been shown [55] that full analysis of such Bell states cannot

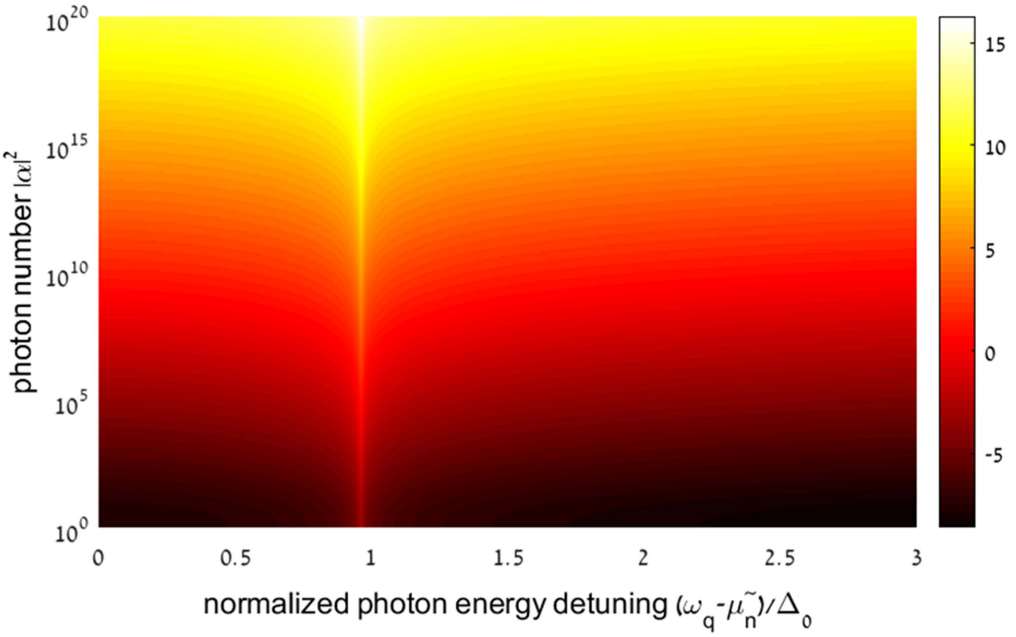


**Figure 7.** Cooper-pair based TPG to OPG gain ratio spectra in the log scale versus photon number $|\alpha_q|^2$ per pulse, based on typical values for III–V semiconductors. Reproduced from [42] © 2016 IOP Publishing Ltd and Deutsche Physikalische Gesellschaft. CC BY 3.0.

be realized through the use of linear optics alone, with conventional nonlinear optical schemes [56] being significantly less efficient.

In the superconductor–semiconductor device approach, efficient Bell-state detection is obtained by inducing superconductivity in a semiconductor photodetector—thus preventing regular one-photon absorption in the superconducting state based on Cooper-pairs, while allowing two-photon absorption. Induced superconductivity forms a BCS state inside the conduction band of the semiconductor (figure 8(a)). In typical direct-bandgap bulk semiconductors, the LH and HH bands, with angular momentum $J_Z^{\mathrm{LH}} = \pm 1/2$ and $J_Z^{\mathrm{HH}} = \pm 3/2$, are degenerate [57], allowing the absorption of various two-photon states with different polarizations. Both LH and HH bands can each separately absorb $|\Psi^{\pm}\rangle$ states, while combinations of holes from both bands give rise to absorption of $|\Phi^{\pm}\rangle$ states. However, in a semiconductor QW the LH–HH degeneracy is lifted [36], which allows the detector to distinguish between the $|\Psi^{\pm}\rangle$ and $|\Phi^{\pm}\rangle$ states as it is not possible to combine holes from both bands in order to achieve absorption of the $|\Phi^{\pm}\rangle$ state. Choosing the two-photon energy by means of filtering to match a double excitation from the HH to the superconducting gap in the conduction band allows the absorption of $|\Psi^{+}\rangle$ only, based on energy and total angular momentum conservation alone. Moreover, the BCS state in the CB allows the absorption of only the $|\Psi^{\pm}\rangle$ state, thus granting the ability to detect a single Bell-state while being transparent to the other three states. The superconducting contact induces superconductivity in the n-type side of an avalanche-photo-diode (APD) by means of the proximity effect (figure 8(b)). Thus, when an entangled photon-pair in the $|\Psi^{+}\rangle$ state is absorbed, a Cooper-pair is formed in the n-type side along with a pair of holes, which are then accelerated towards the impact-ionization layer of the APD and initiate an avalanche which results in a macroscopic detection signal.

In order to be able to convert the different Bell-states into the detectable $|\Psi^{+}\rangle$ state, a simple optical scheme based on diffraction gratings, two quarter-wave plates and a half-wave plate has been devised (figure 8(c)).

## 5. QD superconducting light sources

QDs are zero-dimensional structures, typically on the scale of several nanometers (usually a lower bandgap semiconductor embedded in a wider-bandgap semiconductor), which provide three-dimensional quantum confinement resulting in discrete energy levels—acting as artificial atoms [58–62].

Due to the relatively strong Coulomb interaction in a quantum-confined structure, QDs can support both excitonic (bound electron–hole) and biexcitonic (exciton pair) modes [22]. While a single exciton can decay emitting a single photon, biexciton emission is a cascade of two first-order processes, in which the biexciton decays into an exciton while emitting the first photon, followed by the decay of the exciton to the ground state while emitting the second photon. The emitted a pair of photons is polarization-entangled (figures 9(a) and (b)). Such QD biexciton decay sources have been shown to provide on-demand generation of entangled-photon pairs [22]. However, phenomena such as anisotropic electron–hole exchange interaction cause a polarization-dependent energy splitting in the intermediate exciton state (figures 9(c) and (d)), providing which-path information in the energy of the photons in the pair and thus deteriorating the quality of entanglement. The biexciton to exciton photoluminescence (PL) spectrum is shifted to lower energy than the exciton to ground state PL spectrum

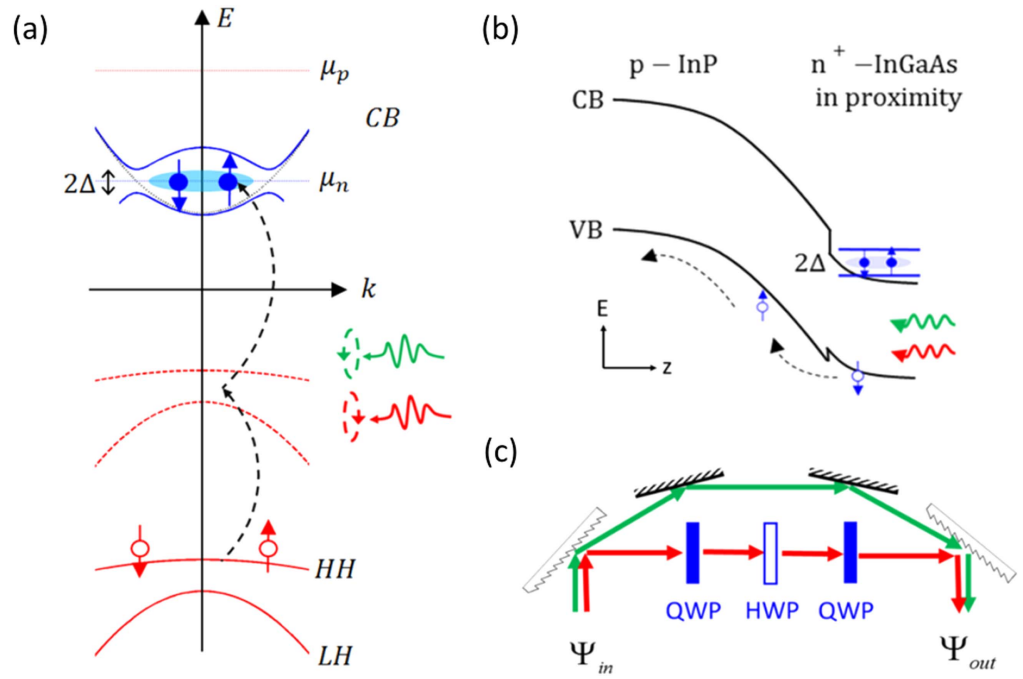


**Figure 8.** (a) Energy band diagram of entangled two-photon absorption in a semiconductor QW superconducting proximity region. Absorption of $|\Psi^{\pm}\rangle$ states is possible from either HH or LH bands while absorption of $|\Phi^{\pm}\rangle$ states is possible through combinations of holes from both hole bands. Such combinations become unlikely as the splitting between both hole bands is increased. (b) Spatial energy band diagram of a standard APD, placed in proximity with a superconductor. (c) An optical scheme converting Bell states into each other. Reprinted figure with permission from [47], Copyright 2017 by the American Physical Society.

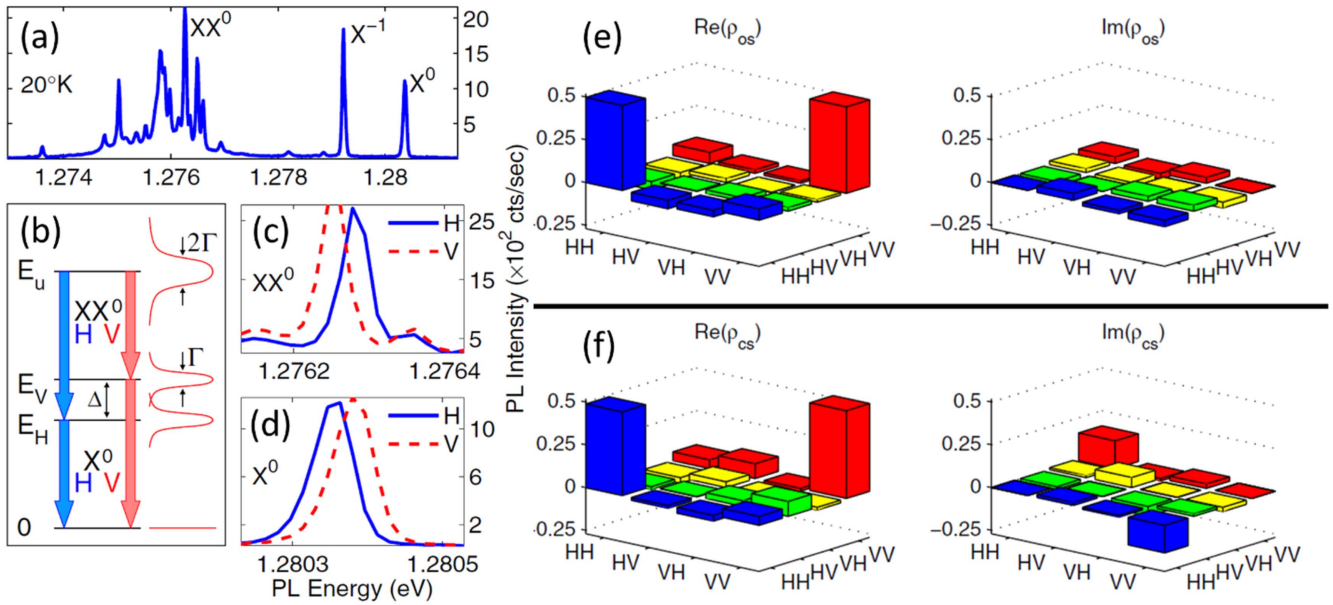


**Figure 9.** (a) Energy spectrum of a single QD. (b) Schematic description of the biexciton cascade. Γ is the radiative linewidth of the exciton level, Δ is the energy splitting between the exciton energy levels, $H$ is the horizontal photon polarization and $V$ is the vertical photon polarization. (c), (d) High resolution polarization-sensitive PL spectra of the biexciton $XX^0$ and exciton $X^0$ lines, respectively. $X^{-1}$ refers to negatively charged trions. (e), (f) The measured two-photon density matrix for photon pairs from a biexciton cascade obtained with a spectral window of (e) 200 $\mu$eV and (f) 25 $\mu$eV. Reprinted figure with permission from [22], Copyright 2006 by the American Physical Society.

(figures 9(c) and (d)) due to the small Coulomb interaction correction which reduces the energy of the biexciton. The energy of the biexciton emission photon is $E_u$–$E_V$ for the vertically polarized photons and $E_u$–$E_H$ for the horizontally polarized photons. While for the exciton decay, the vertical polarization photon energy is $E_V$ and the horizontal polarization photon energy is $E_H$.

This issue has been addressed by several corrective methods. The first group of methods aims to restore symmetries in the QD. This group includes methods such as the

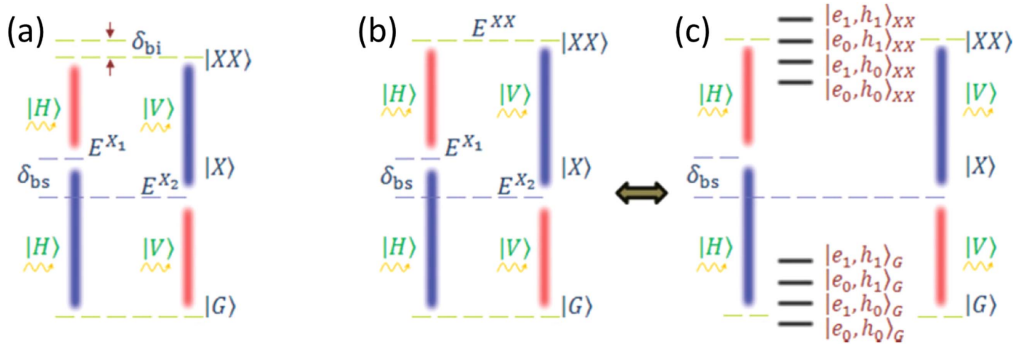


**Figure 10.** (a) Biexciton cascade recombination process with $|H\rangle, |V\rangle$ the horizontal and vertical photon polarizations respectively and $\delta_{bi}$, $\delta_{bs}$ the biexciton binding energy and exciton splitting energy respectively. (b) Biexciton cascade recombination process in the time reordering scheme where $\delta_{bi}$ removed. (c) Biexciton cascade recombination process with superconducting contacts. The QD ground state and the biexcitonic singlet state are split into four levels as a result of being coupled to the BCS coherent state. Reprinted figure with permission from [21], Copyright 2011 by the American Physical Society.

dc or ac Stark effects [63], Zeeman effect [64], thermal and laser annealing [65, 66] and the exploitation of inherent crystal symmetries of III–V nanowire QDs [67]. The second group of methods deals with the emitted photon pairs. This group includes the spectral filtering [22] and time reordering methods [71]. For example, the spectral filtering method is used to filter out the non-entangled parts of the spectrum, thus resulting in a higher degree of entanglement (figures 9(e) and (f)). The density matrix for the photon pair state is [22]:

$$\rho = \begin{pmatrix} |\alpha|^2 & 0 & 0 & \gamma \\ 0 & 0 & 0 & 0 \\ 0 & 0 & 0 & 0 \\ \gamma^* & 0 & 0 & |\beta|^2 \end{pmatrix} \tag{14}$$

with $\alpha$, $\beta$ being the amplitudes of the decay paths and $\gamma$ being an additional off-diagonal parameter. The Peres criterion [68] states that if the off-diagonal parameter $\gamma$ is different from zero, there is a degree of entanglement in the system (figures 9(e) and (f)). For the wide spectral window (figure 9(e)), the off-diagonal term is almost non-existent. This is due to splitting of the intermediate exciton state which results in degradation of entanglement. For the narrow spectral window (figure 9(f)), a clear indication of entanglement can be seen as the off diagonal term $\gamma$ is not zero. The entanglement is stronger as the narrower spectral window filters out the energy different polarizations and leaves only those with similar energy, which are truly entangled.

Nevertheless, fabrication of highly symmetrical QDs still remains a difficult issue while methods such as spectral filtering significantly reduce the entanglement generation rate as well as the probability of on-demand emission. In addition, since QD biexciton decay is a cascaded emission process, it creates a time delay between the biexciton and exciton emission, which may result in decoherence.

It has, therefore, been proposed to couple superconducting contacts to QDs in order to enhance the ability of QDs to emit entangled photon-pairs [20, 21, 69, 70]. This coupling has been shown [21] to induce a fine splitting of both the biexcitonic and ground states into four separate levels (figure 10). The obtained energy structure can then be fine-tuned by applying voltage to the junction so that the biexciton binding energy $\delta_{bi}$ becomes zero. This, in turn, enables the use of the time reordering scheme [71] in order to overcome the exciton splitting energy $\delta_{bs}$ for the generation of pure entangled-photon states.

Other than employing the existing biexciton–exciton decay channel, it has also been suggested [20] that in the case in which the biexciton binding energy is positive, Cooper-pairs injected into the QD will undergo direct recombination with a pair of holes to form an entangled photon-pair. In this case, the enhancement is achieved due to the fact that the injected Cooper-pairs can recombine directly with a pair of holes in a second-order process through a virtual state, to emit entangled-photon pairs. This addresses the intermediate exciton level splitting problem due to mixing by the Bogoliubov transformation and removing which-path information.

A key aspect which has to be considered in the case of QDs is matching between the energy level of the injected Cooper-pairs and the lowest energy level of the QD, since the lack of such matching can cause the injected Cooper-pairs to undergo relaxation and possible breaking of the pairs. There are two key approaches to address this issue. The first is to use a type-I QD (figure 11(a)) whose lowest energy level is aligned with the energy level of the Cooper-pairs so that resonant injection can take place. The second approach uses a type-II QD (figure 11(b)) in which bound states exist only for the hole-like quasiparticles while the Cooper-pairs are injected evanescently into the QD.

As with p–n junction SLED devices, superconducting QD LEDs (SQLEDs) can have either a single superconducting contact on one side of the SQLED, or two superconducting contacts on both sides of the SQLED.

### *5.1. QD SLEDs with a superconducting contact on n-type side only*

Devices of the first type with a single superconducting contact have been successfully implemented [69, 70] and have shown superconductor-related phenomena below $T_c$ such as luminescence intensity enhancement (figures 12(d) and (e)) and

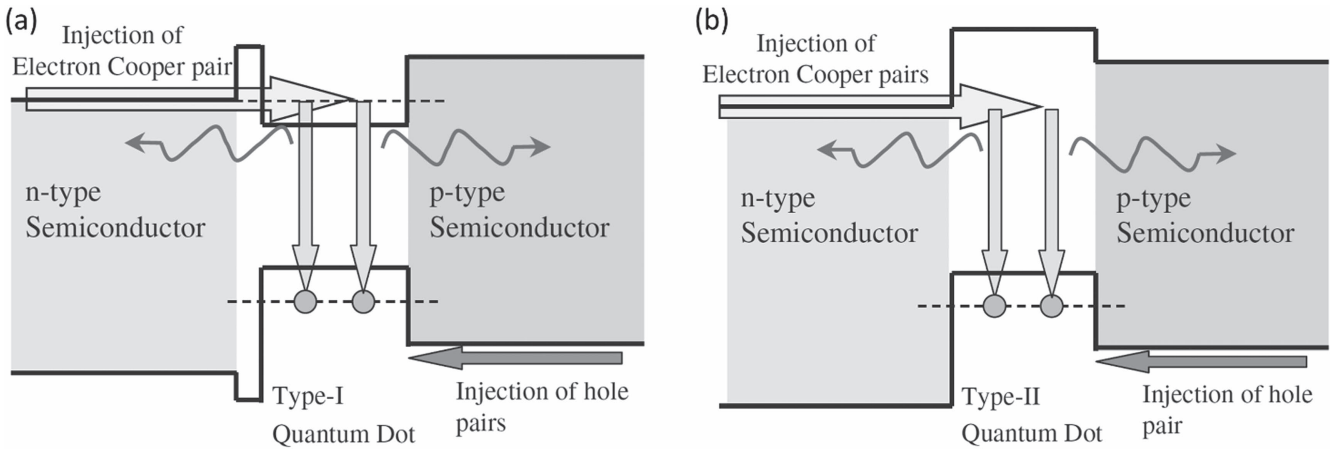


**Figure 11.** (a) Typical structure of a type-I QD. The lowest electron energy level of the QD has to match the Fermi level where the Cooper-pairs reside. (b) Typical structure of a type-II QD. Here, Cooper-pairs are evanescently injected into the QD and then recombine. Reproduced from [20] © 2006 The Japan Society of Applied Physics. All rights reserved.

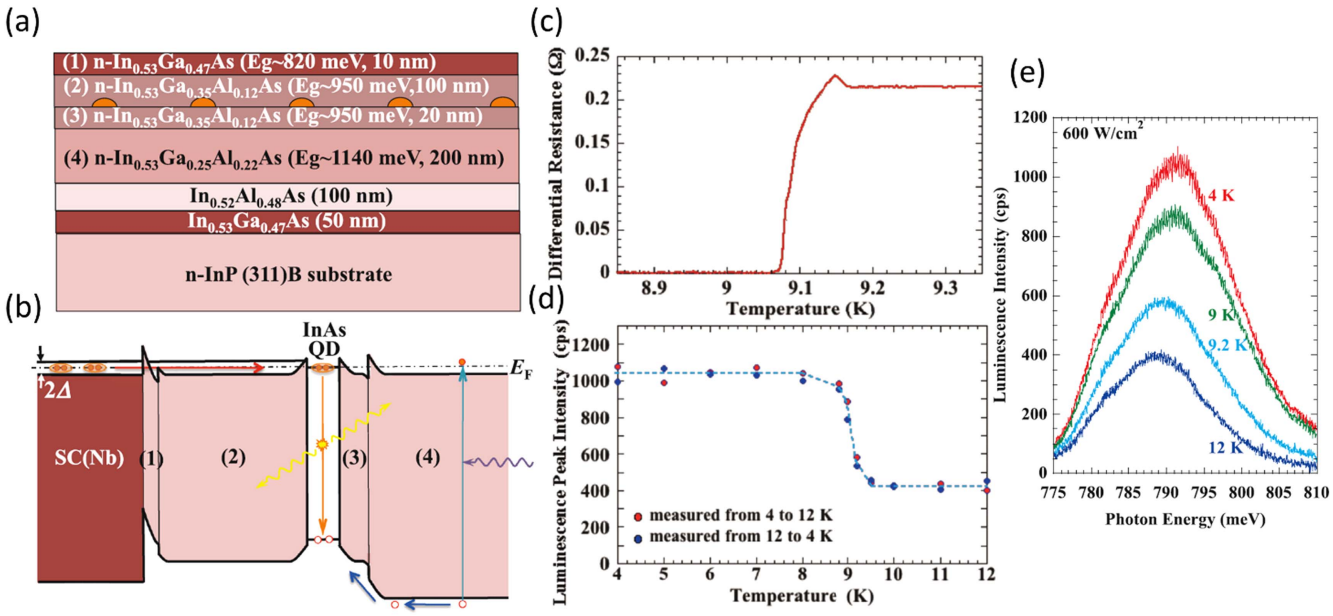


**Figure 12.** (a) Structure scheme of a superconductor-coupled QD device. (b) Energy band scheme of the QD device. Cooper-pairs are injected into the QD through the n-type layers while holes are first excited using a laser and are then injected into the QD. (c) Differential resistance measurement showing Nb transition to superconductivity at ∼9.1 K. (d) Luminescence peak intensity as a function of temperature. An enhancement can be seen below the critical temperature. (e) Spectral luminescence intensity graphs with temperature dependence. Reprinted figure with permission from [70], Copyright 2015 by the American Physical Society.

sharp edges in the emission spectrum superconducting density of states (DOS) [70].

Finally, for both superconductor-coupled QD approaches, since the injected Cooper-pairs are bosons and the hole-like quasiparticles are fermions, control is obtained over the entangled-photon pair generation rate since only two hole-like quasiparticles can populate the lowest hole energy level of the QD.

### *5.2. QD SLEDs with superconducting contacts on both n-type and p-type sides*

Devices of the second type with superconducting contacts on both sides of the device, have also been proposed and studied theoretically. One such example involves two QDs embedded at the center of a p–n junction, which is in turn coupled to superconducting contacts on both sides [72]. In the proposed device, under applied voltage, Cooper-pairs enter the junction and then spatially split, with a single electron entering each QD while still remaining entangled. Each electron then proceeds to recombine with a hole in each QD and emit a single photon, with the two emitted photons being entangled (figure 13(b)).

A more direct approach, which does not require the spatial separation of the electrons composing the Cooper-pair, also exists in the form of QD Josephson junctions, also known as Josephson LEDS (JoLEDs) [18, 73] (figure 13(a)). The application of a voltage $V_{sd}$ across the JoLED results in

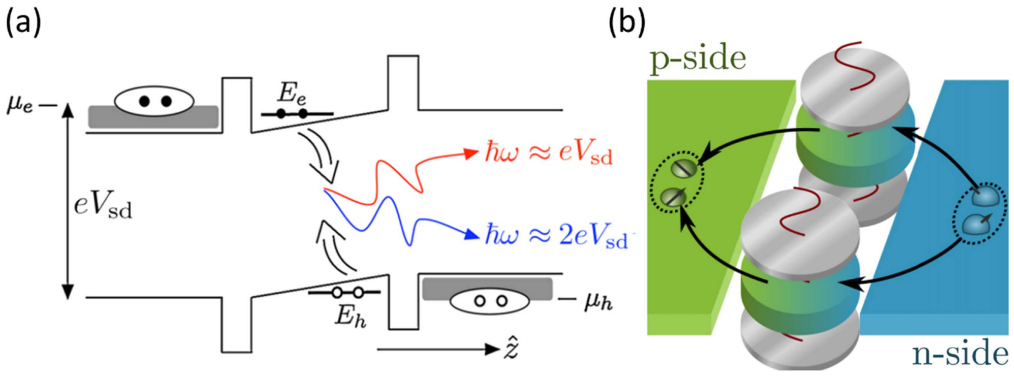


**Figure 13.** (a) A sketch of a QD in contact with two superconducting leads with chemical potentials $\mu_e$, $\mu_h$ and an applied voltage $V_{sd}$. Cooper pairs tunnel into the junction where they recombine to yield either two red photons with energy $eV_{sd}$ or a single blue photon with energy $2eV_{sd}$ where a phonon is created as well. (b) The proposed 2-QD structure which spatially separates the Cooper-pair prior to recombination. (a) Reprinted figure with permission from [18], Copyright 2010 by the American Physical Society. (b) Reprinted figure with permission from [72], Copyright 2010 by the American Physical Society.

Cooper-pairs tunneling into the QD structure to recombine and emit entangled 'red' photon-pairs with energies equal to $eV_{sd}$ each (figure 14(a)). In addition, it has been shown theoretically that an emission of a single 'blue' photon with an energy equal to $2eV_{sd}$ through biexciton decay may also occur (figure 14(b)). Of note is the emitted photon energy dependence on the applied voltage and not on the bandgap. For conventional non-heavily-doped p–n junctions, the important parameter is the bandgap. Since the p–n junction of the JoLED is heavily doped, this is no longer the case as the Fermi levels lie within the bands themselves, so that recombination becomes dependent on the difference between the quasi Fermi levels, determined by the applied voltage. The Hamiltonians responsible for both recombination types are:

$$\widehat{H}_{\text{int},0} = (V_0^{+}\hat{h}_{\downarrow}\hat{c}_{\uparrow} + V_0^{-}\hat{h}_{\uparrow}\hat{c}_{\downarrow})\mathrm{e}^{-\mathrm{i}eV_{\text{sd}}t/\hbar} + \text{h.c},$$
$$\widehat{H}_{\text{int},1} = G\sum_{q}(\hat{a}^{\dagger}_{q,-}\hat{h}_{\downarrow}\hat{c}_{\uparrow} + \hat{a}^{\dagger}_{q,+}\hat{h}_{\uparrow}\hat{c}_{\downarrow})\mathrm{e}^{-\mathrm{i}eV_{\text{sd}}t/\hbar} + \text{h.c}, \quad (15)$$

where $\hat{h}_{\downarrow}$, $\hat{h}_{\uparrow}$ are HH annihilation operators with total angular momentum $j_z = \pm 3/2$, $\hat{c}_{\downarrow}$, $\hat{c}_{\uparrow}$ are electron annihilation operators with angular momentum $j_z = \pm 1/2$, $V_0^{\pm} \propto E_{0,x} \mp \mathrm{i}E_{0,y}$ is a coupling coefficient properties to the applied dc electric field $E_0$, $G$ is a coupling coefficient and $V_{sd}$ is the applied voltage on the junction. The Hamiltonian $\hat{H}_{\text{int},1}$ describes the simple recombination of an electron and a hole while emitting a single photon. Therefore, a second-order perturbation containing just $\hat{H}_{\text{int},1}$ describes the case of two 'red' photons emitted from the device. The Hamiltonian $\hat{H}_{\text{int},0}$ describes the case of non-radiative recombination of an electron an a hole, which is evident as it lack photon creation and annihilation operators. The combination of $\hat{H}_{\text{int},0} + \hat{H}_{\text{int},1}$ can therefore be used to describe the case of 'blue' photon emission as the biexciton first decays non-radiatively to a virtual state, followed by a second radiative decay to the ground state with a 'blue' photon emitted in the process. This is evident by using second-order perturbation theory on the total interaction Hamiltonian and obtaining terms of the form $\hat{H}_{\text{int},0}\hat{H}_{\text{int},1}$ and $\hat{H}_{\text{int},1}\hat{H}_{\text{int},0}$ which yield the single 'blue' photon emission. Since in QDs, particle states are localized, non-radiative decay is more likely as there are no strict constraints on the momentum

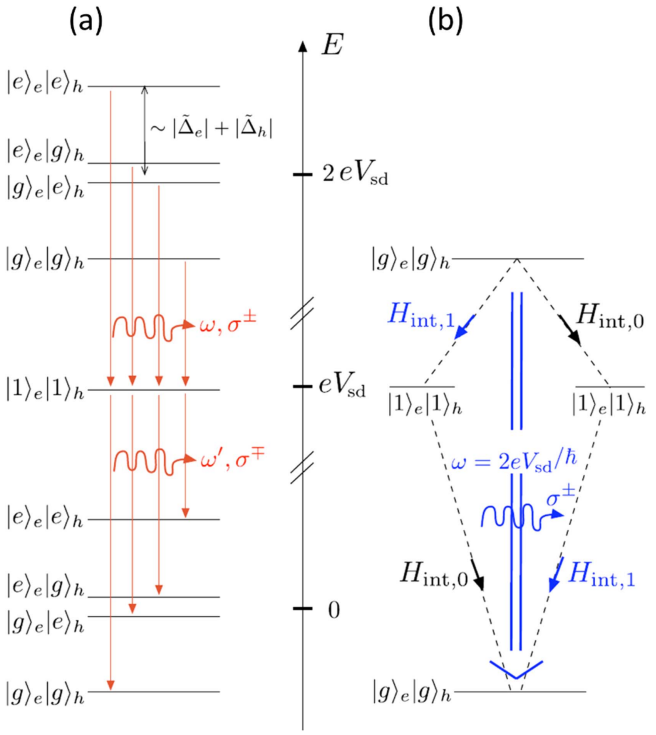


**Figure 14.** (a) Biexciton-exciton recombination diagram with supeconductor induced splitting of the ground and biexciton states. Two 'red' photons with opposite circular polarizations and energy on the order of $eV_{sd}/\hbar$ are emitted. The cascade can proceed via 32 different decay channels which results in eight distinct emission peaks. $\omega$, $\sigma$ are the energy and polarization of the emitted photons respectively and $\tilde{\Delta}_e$, $\tilde{\Delta}_h$ are the induced electron and hole superconducting energy gaps. (b) Recombination diagram for the emission of a 'blue' coherent photon at the Josephson frequency $2eV_{sd}/\hbar$. Reprinted figure with permission from [18], Copyright 2010 by the American Physical Society.

conservation. On the other hand, in bulk and quantum-well based devices, momentum conservation suppresses the nonradiative transitions accompanying the double frequency photon emission.

Other than emitting entangled photon-pairs on demand, the proposed JoLEDs have also been shown to be able to use as 2-qubit gates with qubit manipulation made possible through irradiation pulses and gate-voltage modulation [73].

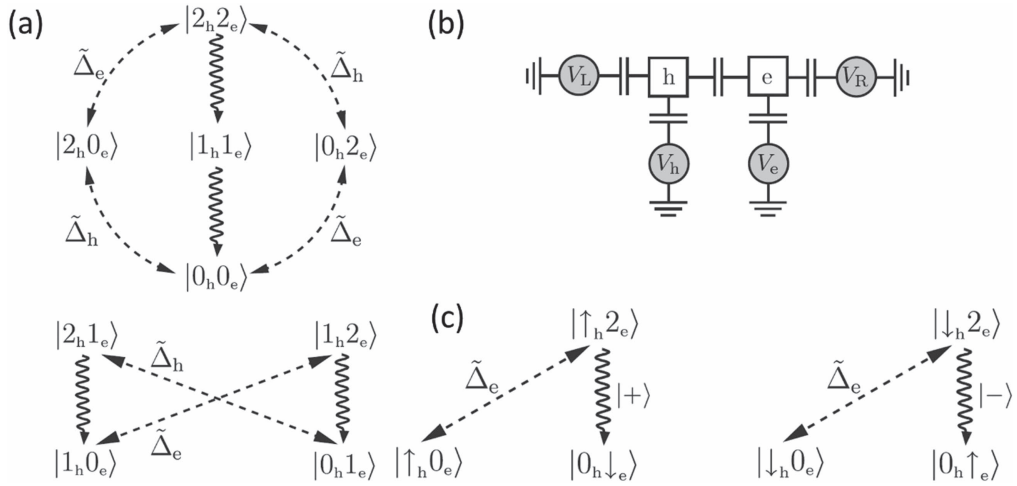


**Figure 15.** (a) Possible electron–hole states (without the spin degree of freedom) along with possible transitions between the states. The upper and lower states are separated as the given processes cannot change the parity of the total number of holes/electrons. The wavy transitions mark electron–hole recombination while the dashed line corresponds to superconductor enabled transitions (formation of electron/hole pairs). (b) 2-qubit capacitance network representation with the two dots $h$, $e$, superconducting leads $V_L$, $V_R$ and gate electrodes $V_h$, $V_e$. (c) The spin measurement process of the initial $|1_h, 0_e\rangle$ state and the emission of a polarized $|+\rangle$ or $|-\rangle$ photon. Reproduced from [73]. 

The 2-qubit system (figure 15(b)) is composed of the $|0_h, 0_e\rangle$, $|2_h, 0_e\rangle$, $|0_h, 2_e\rangle$, $|2_h, 2_e\rangle$ states with the ground state being $|0_h, 0_e\rangle$, these states are separate from the $|2_h, 1_e\rangle$, $|1_h, 0_e\rangle$, $|1_h, 2_e\rangle$, $|0_h, 1_e\rangle$ states (figure 15(a)) since recombination/generation processes only form pairs of particles (electron–electron/electron–hole/hole–hole).

Applying irradiation of frequency $\omega$ to the energy difference between the states sets the required transition. The enabling of transition is made possible by modulation of the contact voltages $V_R$, $V_L$ and QD back gate voltages $V_h$, $V_e$ with the following induced change:

$$\frac{\delta\varepsilon_h}{e} = a_{hh}(V_h - V_L) + a_{he}(V_e - V_L) + a_h(V_R - V_L),$$
$$\frac{\delta\varepsilon_e}{e} = a_{ee}(V_e - V_R) + a_{eh}(V_h - V_R) + a_h(V_L - V_R), \quad (16)$$

where the various a coefficients are obtained from voltages division in the capacitance network (figure 14). The matrix element which facilitates the transitions is $\left|\frac{\hat{\Delta}\delta\varepsilon}{\hbar\omega}\right|$. The readout is made through radiative decay of the $|2_h, 2_e\rangle$ state as it is the only state with a sizable radiative decay time, and while only this state is readable, one can still perform any unitary operation in Hilbert-space prior to the readout.

Moreover, spin measurement can also be made possible through the transfer of the particle's spin into the polarization of the photon. For example, starting from the $|1_h, 0_e\rangle$ state, one can use the conversion process (figure 15(c)) to obtain the $|1_h, 2_e\rangle$ state which then decays to the $|0_h, 1_e\rangle$ state while emitting a polarized photon.

## 6. Half Josephson lasers

The half Josephson laser (HJL) [19] is novel superconducting laser concept based on placing the JoLED inside an optical cavity. Application of voltage across the junction leads to the emissions of 'blue' photons at the Josephson frequency $\omega_J = \frac{2eV_{sd}}{\hbar}$ but also 'red' photons at a frequency $\frac{\omega_J}{2}$ (due to electron–hole recombination), with emphasis placed on the 'red' photons. In ordinary lasers, a coherent photon state is formed through stimulated emission of photons inside a cavity, with the resulting coherent light having a defined optical phase. In HJLs, the optical phase is directly coupled to the superconductor phase difference between the superconducting contacts. The coupling is achieved since the frequency of the emitted 'red' photons is $\frac{\omega_J}{2}$ depends on the applied voltage with the cavity itself designed to match this frequency. This way, the applied voltage is directly coupled to the frequency of the emitted light.

One of the most widely used devices composed of Josephson junctions is the SQUID. SQUIDs are devices composed of two Josephson junctions situated in parallel to each other, while connected at both edges. This setup effectively forms a loop, through which magnetic flux can be measured with high accuracy. In addition, the critical current of the SQUID periodically depends on the magnetic flux flowing through the loop, thus turning the SQUID into a flux-tunable Josephson junction.

Replacing the regular Josephson junctions with JoLEDs was recently proposed [74]. Since JoLEDs feature control over the optical phase of the laser through the superconductor phase difference between its contacts, magnetic flux flowing through the SQUID, changing the superconductor phase difference, can be used to control the optical phase of the resulting laser. In the case of a pair of optically uncoupled HJLs in a SQUID, the optical interference of the light emitted from the pair of HJLs would depend periodically on the magnetic flux, yielding an optical analog of the Aharonov–Bohm effect. Optical coupling can be included, resulting in devices known as light-superconducting interference devices (LSIDs).

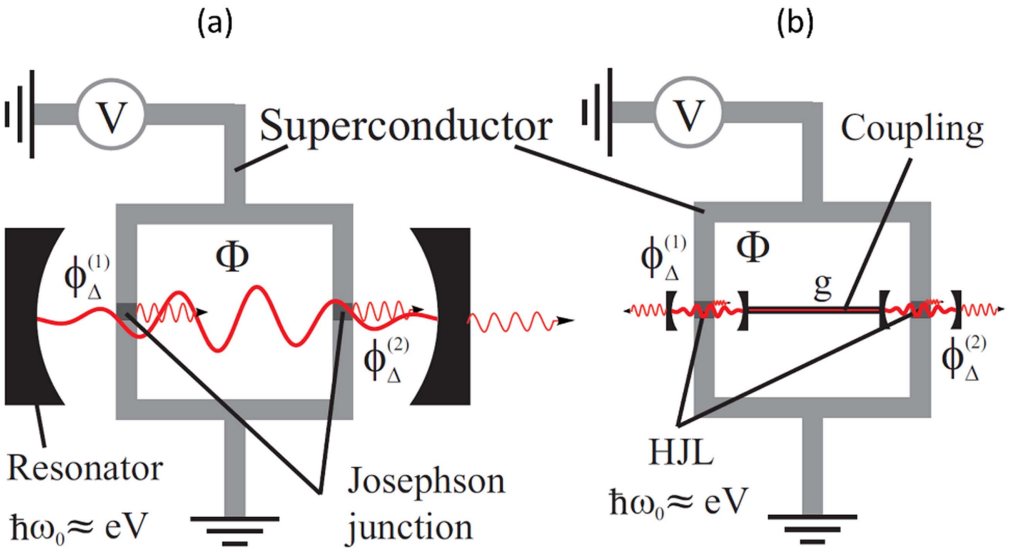


**Figure 16.** A sketch of the two proposed Josephson configurations. (a) Represents the single resonator configuration while (b) represents the double-coupled resonator configuration. Reprinted figure with permission from [74], Copyright 2014 by the American Physical Society.

LSIDs can have two types of optical coupling (figure 16): a single cavity shared by both HJLs having a single resonant mode (single-mode LSID), or two coupled cavities, each with its own resonant mode (two-mode LSID). Such devices not only offer the interesting notion of controlling the lasing with magnetic flux, but also offer an option to generate modulated light. Moreover, the concept of the LSID can be readily expanded to include an arbitrary number of modes, or include various setups in one, two or three-dimensions, with forms similar to those of Josephson junction arrays.

## 7. Summary and outlook

To summarize, the coupling between superconductors and semiconductors has been shown to open a wide range of new directions in the field of optoelectronic devices. Coupling superconducting contacts to QDs have been shown not only to deliver enhanced luminescence at temperatures below $T_c$, but also to achieve enhanced photon-entanglement purity due to their ability to overcome the excitonic energy level splitting. In addition, device concepts such as the SLEDs can offer simple and efficient sources for entangled photons based on semiconductor QWs. A new concept of a Josephson laser could offer accurate control over the optical phase of a laser through the voltage applied on the Josephson junction. The combination of such lasers as LSIDs has been shown to have interesting applications in the field of light modulation.

Moreover, hybrid devices can greatly contribute to the field of quantum information. Superconductor coupled QDs and SLEDs offer enhanced generation of entangled photons. While additional hybrid device concepts such as the two-photon amplifying waveguide and Bell-state analyzer, can also provide a complete infrastructure for quantum information processing and quantum communications. Other than entanglement, hybrid devices such as the Josephson LED, can fulfill the role of both qubits and gates as well as provide the means of measuring spin of single particles.

While this field has grown rapidly in the recent years, it is still an emerging topic. Hybrid semiconductor–superconductor devices carry two major advantages: the first is ability to rapidly integrate them within existing systems due to their compatibility with semiconductors and the vast fabrication knowledge. The second advantage is the discovery of high-$T_c$ superconductors with critical temperatures exceeding the boiling temperature of nitrogen (77 K). Integration of high-$T_c$ superconductors can lead to widespread use of superconductor–semiconductor optoelectronic devices, paving the way for an even broader range of applications in quantum and classical technologies.

## References

[1] Yu P Y and Cardona M 2010 *Fundamentals of Semiconductors* (Berlin: Springer)
[2] Tinkham M 1996 *Introduction to Superconductivity* 2nd edn (New York: McGraw-Hill)
[3] Miller A J, Nam S W, Martinis J M and Sergienko A V 2003 Demonstration of a low-noise near-infrared photon counter with multiphoton discrimination *Appl. Phys. Lett.* **83** 791
[4] Takesue H, Nam S W, Zhang Q, Hadfield R H, Honjo T, Tamaki K and Yamamoto Y 2007 Quantum key distribution over a 40 dB channel loss using superconducting single-photon detectors *Nat. Photon.* **1** 343
[5] Blais A, Huang R-S, Andreas Wallraff, Girvin S M and Schoelkopf R J 2004 Cavity quantum electrodynamics for superconducting electrical circuits: an architecture for quantum computation *Phys. Rev.* A **69** 062320
[6] Clarke J and Wilhelm F K 2008 Superconducting quantum bits *Nature* **453** 1031
[7] Guéron S, Pothier H, Birge N O, Esteve D and Devoret M H 1996 Superconducting proximity effect probed on a mesoscopic length scale *Phys. Rev. Lett.* **77** 3025

[8] van Son P C, van Kempen H and Wyder P 1987 New method to study the proximity effect at the normal-metal–superconductor interface *Phys. Rev. Lett.* **59** 2226

[9] Kastalsky A, Kleinsasser A W, Greene L H, Bhat R, Milliken F P and Harbison J P 1991 Observation of pair currents in superconductor–semiconductor contacts *Phys. Rev. Lett.* **67** 3026

[10] Nguyen C, Kroemer H and Hu E L 1992 Anomalous andreev conductance in InAs–AlSb quantum well structures with Nb electrodes *Phys. Rev. Lett.* **69** 2847

[11] Nishino T, Hatano M, Hasegawa H, Kure T and Murai F 1990 Carrier reflection at the superconductor–semiconductor boundary observed using a coplanar-point-contact injector *Phys. Rev.* B **41** 7274(R)

[12] Heslinga D R, Shafranjuk S E, van Kempen H and Klapwijk T M 1994 Observation of double-gap-edge Andreev reflection at Si/Nb interfaces by point-contact spectroscopy *Phys. Rev.* B **49** 10484

[13] De Franceschi S, Kouwenhoven L, Schönenberger C and Wernsdorfer W 2010 Hybrid superconductor–quantum dot devices *Nat. Nanotechnol.* **5** 703

[14] Katsaros G, Spathis P, Stoffel M, Fournel F, Mongillo M, Bouchiat V, Lefloch F, Rastelli A, Schmidt O G and De Franceschi S 2010 Hybrid superconductor–semiconductor devices made from self-assembled SiGe nanocrystals on silicon *Nat. Nanotechnol.* **5** 458

[15] Sasakura H *et al* 2011 Enhanced photon generation in a Nb/n-InGaAs/p-InP superconductor/semiconductor-diode light emitting device *Phys. Rev. Lett.* **107** 157403

[16] Suemune I *et al* 2010 A cooper-pair light-emitting diode: temperature dependence of both quantum efficiency and radiative recombination lifetime *Appl. Phys. Express* **3** 054001

[17] Asano Y, Suemune I, Takayanagi H and Hanamura E 2009 Luminescence of a cooper pair *Phys. Rev. Lett.* **103** 187001

[18] Recher P, Nazarov Y V and Kouwenhoven L P 2010 Josephson light-emitting diode *Phys. Rev. Lett.* **104** 156802

[19] Godschalk F, Hassler F and Nazarov Y V 2011 Proposal for an optical laser producing light at half the Josephson frequency *Phys. Rev. Lett.* **107** 073901

[20] Suemune I *et al* 2006 Superconductor-based quantum-dot light-emitting diodes: role of cooper pairs in generating entangled photon pairs *Japan. J. Appl. Phys.* **45** 9264

[21] Khoshnegar M and Majedi A H 2011 Entangled photon pair generation in hybrid superconductor–semiconductor quantum dot devices *Phys. Rev.* B **84** 104504

[22] Akopian N, Lindner N H, Poem E, Berlatzky Y, Avron J, Gershoni D, Gerardot B D and Petroff P M 2006 Entangled photon pairs from semiconductor quantum dots *Phys. Rev. Lett.* **96** 130501

[23] Coldren L A 1995 *Diode Lasers and Photonic Integrated Circuits* 2nd edn (New York: Wiley)

[24] Hayat A, Ginzburg P and Orenstein M 2008 Observation of two-photon emission from semiconductors *Nat. Photon.* **2** 238

[25] Hayat A, Ginzburg P and Orenstein M 2009 Measurement and model of the infrared two-photon emission spectrum of GaAs *Phys. Rev. Lett.* **103** 023601

[26] Lin Z and Vuckovic J 2010 Enhanced two-photon processes in single quantum dots inside photonic crystal nanocavities *Phys. Rev.* B **81** 035301

[27] Nevet A, Berkovitch N, Hayat A, Ginzburg P, Ginzach S, Sorias O and Orenstein M 2010 Plasmonic nano-antennas for broadband enhancement of two-photon emission from semiconductors *Nano Lett.* **10** 1848

[28] Hayat A, Ginzburg P and Orenstein M 2007 High-rate entanglement source via two-photon emission from semiconductor quantum wells *Phys. Rev.* B **76** 035339

[29] Hayat A, Nevet A and Orenstein M 2009 Electrically induced two-photon transparency in semiconductor quantum wells *Phys. Rev. Lett.* **102** 183002

[30] Inoue R, Takayanagi H, Akazaki T, Tanaka K, Sasakura H and Suemune I 2014 Carrier flow and nonequilibrium superconductivity in superconductor-based LEDs *Appl. Phys. Express* **7** 073101

[31] Takayanagia H, Inoueb R, Akazaki T, Tanaka K and Suemune I 2010 Superconducting transport in an LED with Nb electrodes *Physica* C **470** 814

[32] Inoue R, Takayanagi H, Akazaki T, Tanaka K and Suemune I 2010 Transport characteristics of a superconductor-based LED *Supercond. Sci. Technol.* **23** 034025

[33] McMillan W L 1968 Tunneling model of the superconducting proximity effect *Phys. Rev.* **175** 537

[34] Sze S M and Ng K K 2006 *Physics of Semiconductor Devices* 3rd edn (New York: Wiley)

[35] Scully M O 1997 *Quantum Optics* 1st edn (Cambridge: Cambridge University Press)

[36] Hayat A, Kee H Y, Burch K S and Steinberg A M 2014 Cooper-pair-based photon entanglement without isolated emitters *Phys. Rev.* B **89** 094508

[37] Josephson B D 1974 The discovery of tunneling supercurrents *Rev. Mod. Phys.* **46** 251

[38] Baireuther P, Orth P P, Vekhter I and Schmalian J 2014 Manipulation of a two-photon pump in superconductor–semiconductor heterostructures *Phys. Rev. Lett.* **112** 077003

[39] Hlobil P and Orth P P 2015 Luminescence and squeezing of a superconducting light-emitting diode *Phys. Rev.* B **91** 205303

[40] Carmichael H J, Milburn G J and Walls D F 1983 Squeezing in a detuned parametric amplifier *J. Phys. A: Math. Gen.* **17** 469

[41] Esaki L and Miyahara Y 1960 A new device using the tunneling process in narrow junctions *Solid-State Electron.* **1** 1

[42] Marjieh R, Sabag E and Hayat A 2016 Light amplification in semiconductor–superconductor structures *New J. Phys.* **18** 023019

[43] Nevet A, Hayat A and Orenstein M 2010 Ultrafast pulse compression by semiconductor two-photon gain *Opt. Lett.* **35** 3877

[44] Marti D H, Dupertuis M-A and Deveaud B 2003 Feasibility study for degenerate two-photon gain in a semiconductor microcavity *IEEE J. Quantum Electron.* **39** 1066

[45] Nevet A, Hayat A and Orenstein M 2010 Measurement of optical two-photon gain in electrically pumped AlGaAs at room temperature *Phys. Rev. Lett.* **104** 207404

[46] Heatley D R, Firth W J and Ironside C N Ultrashort-pulse generation using two-photon gain *Opt. Lett.* **18** 6281993 Ironside C N 1992 Two-photon gain semiconductor amplifier *IEEE J. Quantum Electron.* **28** 842

[47] Sabag E, Bouscher S and Marjieh R 2017 Photonic Bell-state analysis based on semiconductor–superconductor structures *Phys. Rev.* B **95** 094503

[48] White A G, James D F V, Eberhard P H and Kwiat P G 1999 Nonmaximally entangled states: production, characterization, and utilization *Phys. Rev. Lett.* **83** 3103

[49] Boyd R W 2008 *Nonlinear Optics* 3rd edn (London: Academic)

[50] James D F V, Kwiat P G, Munro W J and White A G 2001 Measurement of qubits *Phys. Rev.* A **64** 052312

[51] Rozema L A, Wang C, Mahler D H, Hayat A, Steinberg A M, Sipe J E and Liscidini M 2015 Characterizing an entangled-photon source with classical detectors and measurements *Optica* **2** 430

[52] Bouwmeester D, Pan J W, Mattle K, Eibl M, Weinfurter H and Zeilinger A 1997 Experimental quantum teleportation *Nature* **390** 575

[53] Furusawa A, Sørensen J L, Braunstein S L, Fuchs C A, Kimble H J and Polzik E S 1998 Unconditional quantum teleportation *Science* **282** 706
[54] Briegel H J, Dur W, Cirac J I and Zoller P 1998 Quantum repeaters: the role of imperfect local operations in quantum communication *Phys. Rev. Lett.* **81** 5932
[55] Vaidman L and Yoran N 1999 Methods for reliable teleportation *Phys. Rev.* A **59** 116
[56] Hayat A, Ginzburg P and Orenstein M 2009 Photon energy entanglement characterization by electronic transition interference *Opt. Express* **17** 21280
[57] Lee C C and Fan H Y 1974 Two-photon absorption with exciton effect for degenerate valence bands *Phys. Rev.* B **9** 3502
[58] Ledentsov N N, Ustinov V M, Shchukin V A, Kop'ev P S and Alferov Z I 1998 Quantum dot heterostructures: fabrication, properties, lasers *Semiconductors* **32** 343
[59] Ashoori R C 1996 Electrons in artificial atoms *Nature* **379** 413
[60] Schedelbeck G, Wegscheider W, Bichler M and Abstreiter G 1997 Coupled quantum dots fabricated by cleaved edge overgrowth: from artificial atoms to molecules *Science* **278** 1792
[61] Buluta I, Ashhab S and Nori F 2011 Natural and artificial atoms for quantum computation *Rep. Prog. Phys.* **74** 10
[62] Hawrylak P 1999 Excitonic artificial atoms: engineering optical properties of quantum dots *Phys. Rev.* B **60** 5597
[63] Gerardot B D, Seidl S, Dalgarno P A, Warburton R J, Granados D, Garcia J M, Kowalik K and Krebs O 2007 Manipulating exciton fine structure in quantum dots with a lateral electric field *Appl. Phys. Lett.* **90** 041101
Coish W A and Gambetta J M 2009 Entangled photons on demand: erasing which-path information with sidebands *Phys. Rev.* B **80** 241303(R)
[64] Stevenson R M, Young R J, Atkinson P, Cooper K, Ritchie D A and Shields A J 2006 A semiconductor source of triggered entangled photon pairs *Nature* **439** 179
Stevenson R M, Young R J, See P, Gevaux D G, Cooper K, Atkinson P, Farrer I, Ritchie D A and Shields A J 2006 Magnetic-field-induced reduction of the exciton polarization splitting in InAs quantum dots *Phys. Rev.* B **73** 033306
[65] Rastelli A, Ulhaq A, Kiravittaya S, Wang L, Zrenner A and Schmidt O 2007 *In situ* laser microprocessing of single self-assembled quantum dots and optical microcavities *Appl. Phys. Lett.* **90** 073120
[66] Seguin R, Schliwa A, Germann T D, Rodt S and Potschke K ¨ Strittmatter A, Pohl U W, Bimberg D, Winkelnkemper M, Hammerschmidt T and Kratzer P 2006 Control of fine-structure splitting and excitonic binding energies in selected individual InAs/GaAsInAs/GaAs quantum dots *Appl. Phys. Lett.* **89** 263109
[67] Singh R and Bester G 2009 Nanowire quantum dots as an ideal source of entangled photon pairs *Phys. Rev. Lett.* **103** 063601
[68] Peres A 1996 Separability criterion for density matrices *Phys. Rev. Lett.* **77** 1413
[69] Mou S S, Irie H, Asano Y, Akahane K, Kurosawa H, Nakajima H, Kumano H, Sasaki M and Suemune I 2015 Superconducting light-emitting diodes *IEEE J. Sel. Top. Quantum Electron.* **21** 7900111
[70] Mou S S, Irie H, Asano Y, Akahane K, Nakajima H, Kumano H, Sasaki M, Murayama A and Suemune I 2015 Optical observation of superconducting density of states in luminescence spectra of InAs quantum dots *Phys. Rev.* B **92** 035308
[71] Avron J E, Bisker G, Gershoni D, Lindner N H, Meirom E A and Warburton R J 2008 Entanglement on demand through time reordering *Phys. Rev. Lett.* **100** 120501
[72] Schroer A and Recher P 2015 Detection of nonlocal spin entanglement by light emission from a superconducting p–n junction *Phys. Rev.* B **92** 054514
[73] Hassler F, Nazarov Y V and Kouwenhoven L P 2010 Quantum manipulation in a Josephson light-emitting diode *Nanotechnology* **21** 274004
[74] Godschalk F and Nazarov Y V 2014 Light-superconducting interference devices *Phys. Rev.* B **89** 104502